Dissociative recombination cross section and branching ratios of protonated dimethyl disulfide and *N*-methylacetamide

A. Al-Khalili, R. Thomas, A. Ehlerding, F. Hellberg, W. D. Geppert, V. Zhaunerchyk, M. af Ugglas, and M. Larsson
Department of Physics, Stockholm University, Alba Nova, SE-106 9I Stockholm, Sweden

E. Uggerud, J. Vedde, and C. Adlhart
Department of Chemistry, University of Oslo, N-0315 Oslo, Norway

J. Semaniak and M. Kamińska
Institute of Physics, Świętokrzyska Academy, ul. Świętokrzyska 15, PL-25406 Kielce, Poland

R. A. Zubarev and F. Kjeldsen
BioMedical Center, Uppsala University, SE-751 23 Uppsala, Sweden

P. U. Andersson
Department of Chemistry, Atmospheric Science, Göteborg University, SE-412 96 Göteborg, Sweden

F. Österdahl
Department of Physics, Royal Institute of Technology, Alba Nova, SE-106 91 Stockholm, Sweden

V. A. Bednarska
Faculty of Sciences, University of Nijmegen, Nijmegen, The Netherlands

A. Paál
Manne Siegbahn Laboratory, Frescativägen 24, SE-104 05 Stockholm, Sweden

(Received 30 April 2004; accepted 23 June 2004)

Dimethyl disulfide (DMDS) and *N*-methylacetamide are two first choice model systems that represent the disulfide bridge bonding and the peptide bonding in proteins. These molecules are therefore suitable for investigation of the mechanisms involved when proteins fragment under electron capture dissociation (ECD). The dissociative recombination cross sections for both protonated DMDS and protonated *N*-methylacetamide were determined at electron energies ranging from 0.001 to 0.3 eV. Also, the branching ratios at 0 eV center-of-mass collision energy were determined. The present results give support for the indirect mechanism of ECD, where free hydrogen atoms produced in the initial fragmentation step induce further decomposition. We suggest that both indirect and direct dissociations play a role in ECD. © *2004 American Institute of Physics.* [DOI: 10.1063/1.1782772]

I. INTRODUCTION

Dissociative ion-electron recombination (DR) on large multiply charged biomolecules has a high potential for routine application in the rapidly growing area of proteomics. This method, usually termed electron capture dissociation (ECD) for biomolecular ions, has proven to be highly efficient in fragmenting large proteins, thereby complementing and augmenting the most commonly used method for the purpose of protein and peptide sequencing of collision induced dissociation (CID).[1–5] In contrast to CID spectra[6–9] which typically exhibit cleavage of the peptide bond, the C_O-N bond, the fragments produced in ECD derive mainly from cleavage of the bond next to the peptide bond, namely, the bond between the alpha carbon and the nitrogen, the N-C_α bond. Furthermore ECD has been shown to be a useful tool for localizing posttranslational modifications, such as disulfide bridges.[2] These observations have raised questions concerning the fragmentation mechanisms involved in the ECD process. Two mechanisms have been suggested.[1,2,10–12] For simplicity, these are called the direct and indirect processes. In the direct process, the protonated site of the protein becomes highly excited after capturing an electron, and the capture is then stabilized through dissociation. The thermochemically preferred dissociation channel proceeds usually via breakup of the C_α-N bond:[13,14]

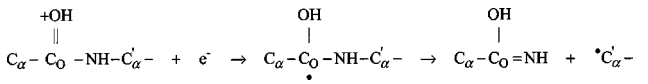

(1)

However, this mechanism does not necessarily explain fragmentation of disulfide bridges present in folded proteins, since it is less likely that the proton is directly attached to the disulfide bond. The high hydrogen affinity of a disulfide bridge suggests that an indirect process could be involved, where the protein releases a hydrogen atom after capturing an electron. This hydrogen atom may then either collide with the disulfide bridge [Eq. (2)] or with the oxygen of the amide bond [Eq. (3)] resulting in cleavage of the disulfide bond or the amine bond, respectively,

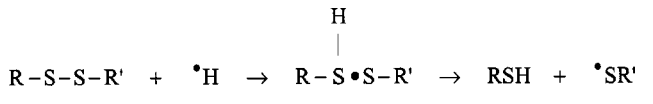

(2)

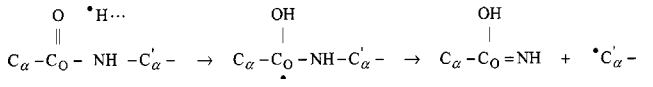

(3)

In order to investigate these two mechanisms we need model systems having the key functional groups (disulfide bridge and a representative portion of a peptide chain), without being too complex. Such systems are dimethyl disulfide (DMDS) and *N*-methylacetamide ($CH_3CONHCH_3$), respectively. One should notice that *N*-methylacetamide has both C_O-N and N-C_α bonds, making it a perfect choice for comparing the dissociation channels arising from cleavage of these bonds. In an attempt to distinguish between the two methyl groups, the acetyl methyl group was fully deuterated. Since the ionization of the proteins studied in the ECD process is likely to be due to protonation, the DMDS and *N*-methylacetamide ions have to be protonated in order to keep the consistency. However, even if the sulfur bridges in protein are less likely to be protonated, a much higher DR cross section as well as dominant S-S bond cleavage branching ratio could suggest that the direct mechanism is involved.

For singly charged small molecular ions, an ion storage ring is a very suitable experimental device to perform ion-electron interaction studies, since the ions can be accelerated to high energy (typically a few MeV). The high ion beam energy not only allows the use of a merged electron-ion beam, where collision energies as low as 1 meV can be obtained, but also gives the possibility to use mass sensitive detectors for detecting the neutral fragments produced in the DR process. A number of experimental aspects regarding the use of ion storage rings for electron-molecular ion interaction studies are discussed in Ref. 15.

II. EXPERIMENT AND DATA ANALYSIS

The experiment has been carried out at the heavy-ion storage ring CRYRING (Fig. 1) at the Manne Siegbahn Laboratory in Stockholm. A more detailed description of the experimental details and the data analysis procedure can be found elsewhere.[16,17] However, a brief description is given here. Both ion species were produced in a high-pressure hollow cathode ion source (JIMIS).[18] The ions were produced from a mixture of methanol and DMDS or *N*-methylacetamide-2,2,2-d_3 vapor. *N*-methylacetamide-2,2,2-d_3 was synthesized, according to Ref. 13, to yield 92%. The gas mixture in both cases was ten parts methanol to one part DMDS/*N*-methylacetamid-2,2,2-d_3 with a final pressure of $\sim 10^{-4}$ Torr measured outside the discharge chamber ($\sim$three to four times higher in the discharge chamber). The source was run with a pulsed anode in order to avoid sooting. Furthermore, the source parameters were optimized to minimize the contribution arising from the ^{13}C isotope in the unprotonated ions. The ions were then extracted through a field of 40 kV and mass selected by a dipole magnet. Once

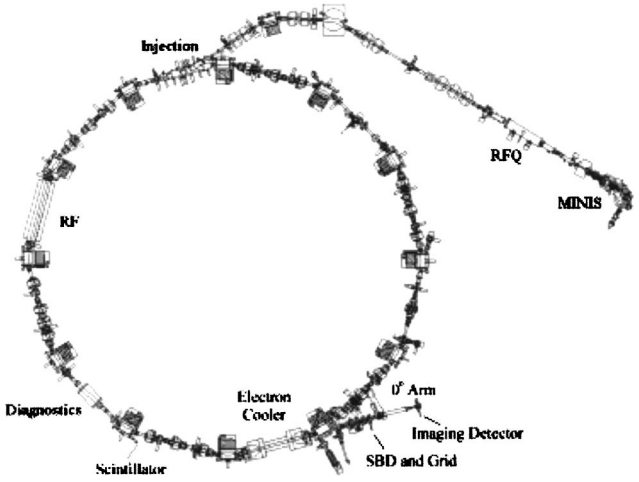

FIG. 1. A schematic of the heavy-ion storage ring CRYRING at the Manne Siegbahn Laboratory at Stockholm University. The ions are merged with an electron beam in the electron cooler section and the neutral fragments arriving from the interaction are detected by the neutral detector.

injected into the ring, the ions were further accelerated in a radio frequency drift tube to an energy of 1 MeV for DMDS and 1.3 MeV for *N*-methylacetamide-2,2,2-d_3. In one of the ring segments the ions were merged with an adiabatically expanded monoenergetic electron beam.[19] These electrons have a velocity distribution that can be described by an anisotropic Maxwell-Boltzmann distribution:

$$f(\overline{v_e}) = \frac{m_e}{2\pi k T_{e\perp}} \sqrt{\frac{m_e}{2\pi k T_{e\parallel}}} \exp\left(-\frac{m_e v_{e\perp}^2}{2kT_{e\perp}} - \frac{m_e v_{e\parallel}^2}{2kT_{\parallel}} \right), \tag{4}$$

where m_e is the electron mass, k is the Boltzmann constant, $v_{e\parallel}$ and $v_{e\perp}$ are the longitudinal and transverse electron velocities, respectively, and $T_{e\parallel} = 0.1$ and $T_{e\perp} = 2$ meV are the longitudinal and transverse electron temperatures, respectively. Initially the electron velocity is set to match the velocity of the ions in order to obtain phase-space cooling. However, due to the heavy mass of the ions as well as the low electron beam current ($\sim 57\ \mu$A) the effect of the phase-space cooling is minimal; hence the ion beam diameter is not shrunk and the beam full width at half maximum is about 1.5 cm. The velocity of the electron can also be changed relative to the ion velocity in order to obtain different center-of-mass collision energy ($E_{\text{c.m.}}$), which is approximated by

$$\sqrt{E_{\text{c.m.}}} = \sqrt{E_{\text{lab}}} - \sqrt{E_{\text{cool}}}, \tag{5}$$

where E_{lab} is the electron energy in the laboratory frame of reference and E_{cool} is the electron energy in the same frame for which the average velocities of the electron and ion beam are matched to each other. Neutral fragments produced in the DR reaction leave the ring tangentially as they are unaffected by the field of the dipole magnet after the electron cooler. These fragments are then detected by a surface barrier detector (SBD). The neutral fragments carry a fraction of the total beam energy proportional to their relative mass. After impinging the detector they yield pulses whose amplitude is proportional to energy carried by them and, thus, to the mass of the fragment. In the reactions studied in this work there

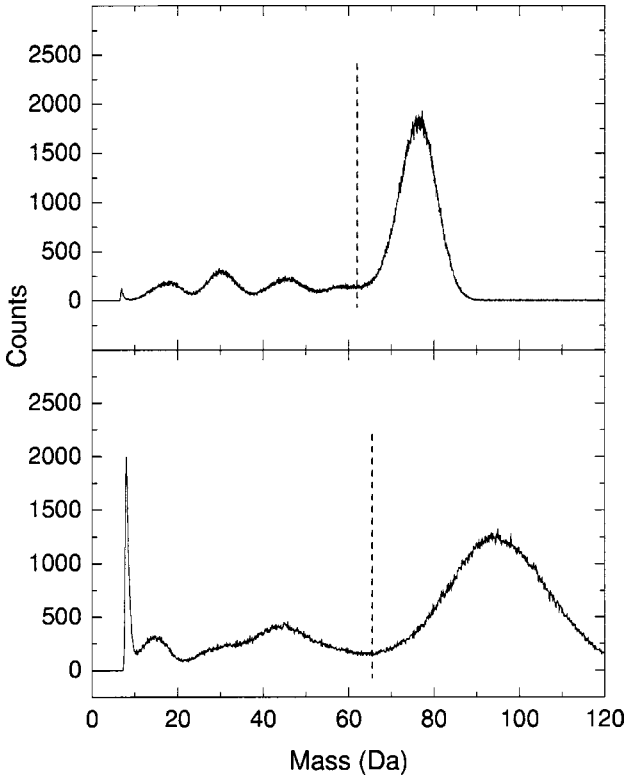

FIG. 2. The energy spectra of the neutral fragments that are produced in DR process of protonated *N*-methylacetamide-2,2,2-d_3 (top) and protonated DMDS (bottom). The dashed lines represent the lower discrimination levels which were used in order to record the DR rate.

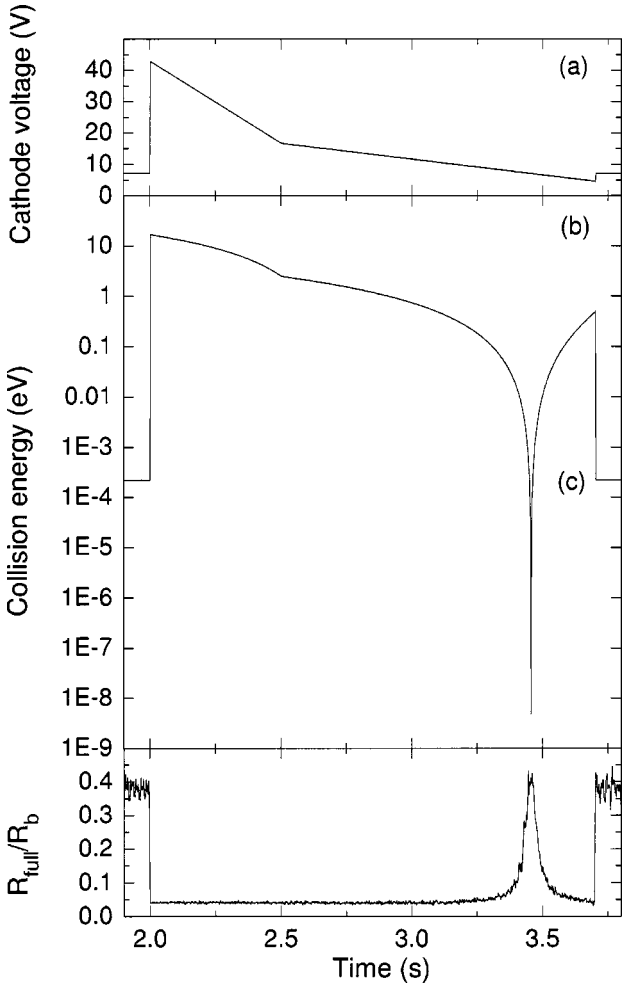

FIG. 3. (a) The electron energy scan as a function of time. (b) The corresponding center-of-mass collision energy as function of time. (c) The ratio between the recorded full beam energy signal and the background rate signal (R_{full}/R_b) as a function of time.

are three different fragmentation processes that contribute to the pulse height spectrum. These processes are

$$AB^+ + e^- \rightarrow A + B \quad (\text{DR}), \tag{6}$$

$$AB^+ + R \rightarrow A + B^+ + R \quad (\text{background destruction}) \tag{7a}$$

$$\rightarrow AB + R^+ \quad (\text{charge transfer}), \tag{7b}$$

where AB is the molecule under investigation and R represents a particle of the residual gas which consists mainly of H_2.

Due to the long integration time of the detector electronics the fragments from one DR event arriving with short difference in time (of the order of nanoseconds) will be detected as one single event with maximum mass, which corresponds to the full beam energy. This is also true for fragments originating from the charge transfer events and therefore the measured spectra have to be corrected for it. Figure 2 shows the pulse height spectra recorded for protonated DMDS and protonated *N*-methylacetamide-2,2,2-d_3 as well as the low discrimination levels that were set to record the DR rate.

A. Cross section

The DR rate was measured by detuning linearly the voltage of the electron gun cathode from maximum value which corresponds to an electron velocity that is higher than that of the ions towards minimum value for which that velocity is lower. The electron cathode voltage and its corresponding center-of-mass energy are shown in Figs. 3(a) and 3(b). Except for the numerical value of the electron cathode voltage the center-of-mass collision energy range investigated for both ion species was the same (0–16 eV). One reason for detuning the electron velocity in this manner is to determine the electron cathode voltage for which the average electron and ion velocities are equal. This occurs when the DR rate signal reaches its highest value. The full beam energy signal (R_{Full}) from the output of the detector electronics was monitored with a multichannel scaler (MCS). Furthermore, a multichannel plate detector located in a different segment of the ring was used together with a second MCS to record the fragments produced in the background collision processes, R_b. To account for the decay of the ion beam R_b is used to normalize the DR rate to the ion current. The ratio between the R_{full} and R_b signals is shown in Fig. 3(c). At the end of acceleration stage in each beam cycle, the rf voltage is held at its maximum value for a short time (minimum 20 ms) to keep the ion beam bunched. During this period the ion beam is measured with a beam charge monitor (BCM) from Bergoz capable of measuring ion currents down to 5 nA with 1 nA rms resolution.[20] As mentioned, the current is needed to

relate the measured R_b to the ion beam decay in order to determine the absolute DR rate coefficient, $\langle v_d\sigma\rangle$, calculated using the following relation:

$$\langle v_d\sigma\rangle = \frac{R_{\mathrm{DR}}}{R_b}\frac{v_i q e}{n_e l}R_{\mathrm{BD}}, \tag{8}$$

where σ is the DR cross section, v_d is center-of-mass velocity, v_i is the velocity of the ions, q is the charge state, e is the elementary charge, l is the interaction length of the electrons with the ions, n_e is the electron density, R_{DR} is the DR rate, and R_{BD} is the background destruction rate per ion per unit time and is given by the ratio between R_b and ion-beam current I. According to the data plotted in Fig. 3(c) the R_{full}/R_b ratio is constant for center-of-mass collision energies above 0.3 eV. Thus the DR contribution to the recorded signal can be neglected for collision energies above 0.3 eV. At these energies the main contribution to R_{full} is from the charge transfer process and part of the background rate cannot be separated from the DR rate due to the low resolution of the detector (see Fig. 2). To correct for these contributions we have assumed that the average signal within the 0.3–2 eV region is a pure background signal, and subtracted this from the total R_{full}/R_b ratio. The reason for selecting this range is to avoid the effect of dissociative excitation, a process occurring at energies higher than 2 eV, which contributes to the background rate signal. R_{DR}, in Eq. (8), then becomes R_{full}-average(R_{full}/R_b) (0.3–2 eV).

The measured DR rate coefficient is related to the cross section by

$$\langle v_d\sigma(v)\rangle = \int_{-\infty}^{\infty} v\,\sigma(v) f(v_d,\overline{v})\,\overline{dv}, \tag{9}$$

where $f(v_d,\overline{v})$ is the electron distribution given in Eq. (1), $v=\sqrt{v_{e\perp}^2+v_{e\|}^2}$, and $\overline{dv}=2\pi v_{e\perp}dv_{e\|}dv_{e\perp}$. If we assume that the cross section is not affected by the transversal electron temperature ($\sim$2 meV) over the energy range 1 meV–0.3 eV, the measured DR cross section $\sigma(v)$ can be written as

$$\sigma(v) = \frac{\langle v_d\sigma(v)\rangle}{v_d}, \tag{10}$$

where v, in this case, is also the detuning velocity v_d.

There are two further corrections that have to be done. The first of these is the space charge correction, which corrects for the radial electron energy change toward the center of the electron beam due to the space charge well created by the electron beam. This energy E is lower in the center of the electron beam and is calculated by iteratively solving the following relation:

$$E = E_{\mathrm{cath}} - \frac{I_e r_c m_e c^2}{e v_e}\left[1+2\ln\left(\frac{b}{a}\right)\right], \tag{11}$$

where E_{cath} is the electron cathode voltage, I_e is the electron beam current, c is the speed of light, r_c is the classical electron radius, m_e is the electron mass, v_e is the electron lab-frame velocity, and b and a are the diameters of the beam tube and electron beam, respectively.

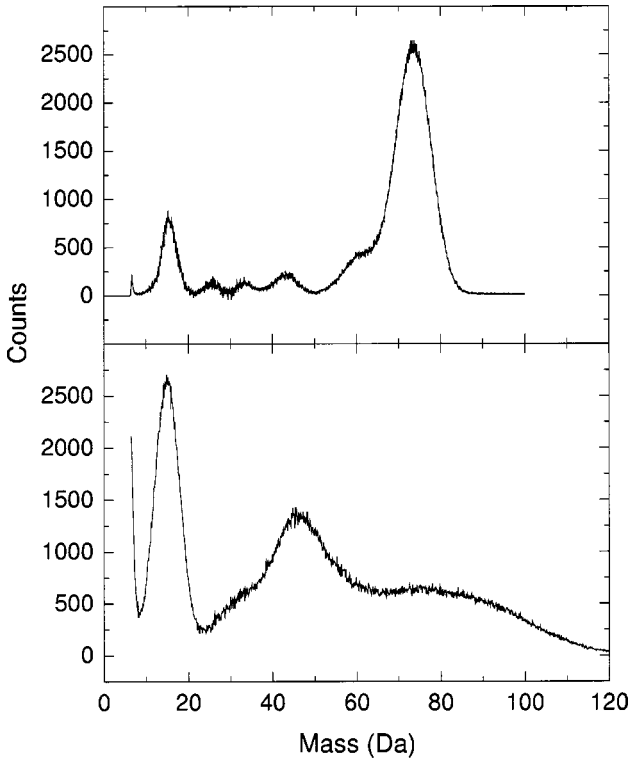

FIG. 4. The background substracted energy spectra of protonated N-methylacetamide-2,2,2-d_3 (top) and protonated DMDS (bottom) taken with 0 eV center-of-mass collision energy and with a transmission grid placed in front of the SBD detector. The signals observed at lower mass are due to DR events that partially pass through the transmission grid.

The second correction is related to the contribution of the electron-ion collisions occurring in the toroidal magnets at both bent sections of the electron cooler, in which the relative collision energies are higher than in the parallel section. This means that the measured DR rate at every collision energy, $[R_{\mathrm{meas}}(E)]$, includes contributions from DR events at higher collision energies. Knowing the geometry of the electron beam, the real rate, R_{real}, can be found by iteratively solving the following relation:

$$R_{\mathrm{real}} = R_{\mathrm{meas}}(E) - \frac{2}{l}\int_0^{x_{\max}} R[E(x)]\,dx, \tag{12}$$

where $E(x)$ is the collision energy at distance x from the edge of the parallel section and $x_{\max}$ is the distance at which the ion and electron beams no longer overlap.

B. Branching ratio

To measure the branching ratios, a stainless grid with a known transmission was placed in front of the SBD. The grid is thick enough to stop those fragments that do not pass through the holes. The probability of a fragment to pass through a hole is equal to the transmission of the grid ($T=0.297$), while the probability of a fragment not to pass is $(1-T)$. Due to the mass difference of the fragments that pass through the detector, the fragments from a DR event will appear at different energy (mass) peaks (see Fig. 4). Since the background peaks will now have a contribution from the DR process, two sets of data are needed in order to

TABLE I. Energies from quantum chemical calculations.

Molecule	B3LYP/6-31G(d), electronic energy (hartree)	B3LYP/6-31G(d), zero-point vibrational energy (hartree)	G2 (0 K), energy (hartree)
H (**1**)	−0.500 273		−0.499 810
CH_3SSCH_3 (**8**)	−876.207 515	0.077 942	−875.124 551
$[CH_3S(SH)CH_3]^+$ (**9**)[a]	−876.516 374	0.087 953	−875.428 652
$CH_3S^*\cdots HSCH_3$ (**10**)[a]	−876.762 296	0.084 737	−875.663 093
10@**9**[a]	−876.687 324		
CH_3S (**11**)	−438.059 725	0.035 850	−437.511 253
CH_3SH (**12**)	−438.698 347	0.046 420	−438.148 469
CH_3 (**4**)			−39.745 086
CH_3SSH (**12**)	−836.889 991	0.048 220	−835.898 094
CH_2S	−437.462 333	0.024 900	−436.933 692
HS* (**4**)	−398.740 028	0.006 097	−398.286 972
CH_2(T) (**9**)			−39.069 013

[a]QCISD(T,E4T)/6-311G(d,p)//MP2(fu)/6-31G(d) energies are **9**: −875.283 355 1, **10**@**9**−: −875.398 323 2, **10**: −875.520 617 2.

subtract the background signal. These data sets are taken at 0 and 2 eV center-of-mass collision energies, respectively. The former of these corresponds to data containing DR +background reactions and the latter to background reactions only. The reason that the electrons are not turned off when taking the background data is that the ion beam is affected by the presence of the electron beam and one needs to have as similar conditions as possible in both cases. Knowing the different exothermic reaction pathways for each ion one can easily set up an equation system to determine the branching ratio. It should also be mentioned that two SBD detectors with different diameters (39 and 61 mm) were used in order to check if fragments are lost off the edges of the detector. The mass spectra taken with these two detectors looked similar, indicating that there are no heavy fragments lost. However, hydrogen atoms are more than likely to be lost, but this will not affect the outcome of the results since, as will be mentioned later, the detector resolution cannot resolve 1 Da mass difference and therefore a grouping of channels is applied to the analysis.

In order to estimate the thermochemistry of possible reaction channels a series of *ab initio* calculations were conducted employing the GAUSSIAN98 suite of programs.[21] First, Becke 3-parameter Lee-Yang-Parr (B3LYP) density functional theory (DFT) calculations were done with the 6-31G(d) basis sets. All minima were subject to a complete geometry optimization, including a check for the correct number of negative Hessian eigenvalues. At this stage, analytical force constants were computed and the vibrational harmonic frequencies were obtained together with the rotational constants. From these calculated spectroscopic constants, zero-point vibrational energies and thermochemical quantities were calculated within the rigid-rotor/harmonic-oscillator approximation. Zero-point vibrational energies were included with appropriate scaling factors.[22] Finally, G2 theory (Ref. 23) calculations were used to obtain the most accurate energy estimates. G2 theory is a compound technique which involves initial geometry optimizations at the HF/6-31G(d) level and subsequent calculation of zero-point vibrational energies (ZPVEs) at the same level of theory. Then the geometry is reoptimized at the MP2(full)/6-31G(d) level whereupon a number of single-point MP2, MP4, and QCISD(T) calculations are performed in order to obtain an energy estimate which is effectively at the QCISD(T)/6-311+G(3df,2p) level. Generally, we found good agreement between the B3LYP and the G2 relative energies (see Table I). On the basis of the G2 energies we find the following exothermic channels for DMDS. These numbers are consistent with those found in Ref. 10:

$$CH_3SSHCH_3^+ + e^-$$

$$\rightarrow CH_3S^* + CH_2S + H^* + H^* + 0.4 \text{ eV} \quad (13a)$$

$$\rightarrow CH_3^* + SH^* + CH_2S + H^* + 1 \text{ eV} \quad (13b)$$

$$\rightarrow CH_3S^* + CH_3S^* + H^* + 2.5 \text{ eV} \quad (13c)$$

$$\rightarrow CH_3^* + SH^* + CH_3S^* + 3.1 \text{ eV} \quad (13d)$$

$$\rightarrow CH_3SH + CH_2S + H^* + 4.2 \text{ eV} \quad (13e)$$

$$\rightarrow CH_3SSCH_3 + H^* + 5.3 \text{ eV} \quad (13f)$$

$$\rightarrow CH_3SSH + CH_3^* + 5.8 \text{ eV} \quad (13g)$$

$$\rightarrow CH_3SH + CH_3S^* + 6.3 \text{ eV}. \quad (13h)$$

Using the QCISD(T,E4T)/6-311G(d,p)//MP2(fu)/6-31G(d) data, we obtain an adiabatic recombination energy for $CH_3SSHCH_3^+$ of 3.1 eV, and a vertical recombination energy of 6.5 eV.

The comparatively low beam energy of fragments in this mass range coupled with the limited resolution of the detector makes it impossible to distinguish fragments that differ in mass by less than 4 Da with full confidence. Due to this situation the dissociation channels listed above were collected into groups depending only on the heavy elements C and S. These dissociation groups are then

$$CSSC^+ + e^- \rightarrow CSS + C \quad (14a)$$

$$\rightarrow CS + CS \quad (14b)$$

$$\rightarrow C + S + CS \quad (14c)$$

$$\rightarrow CSSC. \quad (14d)$$

The contribution from each of these channels to any peak in the data is then described by the linear equation system given below. As an example the contribution to the methyl peak from channel (14a) is $T(1-T)$ where T is the probability for C to pass through and $(1-T)$ is the probability for CSS to be stopped. However, the final analysis is not so straightforward. In the case of channel (14a), for example, which is only connected to channel (13g) from the ungrouped dissociation channels, the procedure mentioned above is trivial. However, we have to include the contribution to methyl group signals arising from channel (14c). Channel (14c) is the grouping of channels (13b) and (13d). The contributions from channels (13b) and (13d) to the methyl signal are given by $T(1-T)^3+T^2(1-T)^2$ and $T(1-T)^2$, respectively. Taking all of these into consideration, the number of counts in the methyl peak, N_C, is now given by

$$N_C = T(1-T)N_{(14a)} + [T(1-T)^3 + T^2(1-T)^2 + T(1-T)^2]N_{(14c)},$$

where $N_{(14a)}$ and $N_{(14c)}$ are the numbers of DR events from the dissociation channels (14a) and (14c), respectively. There are six different mass combinations that can be obtained from the different dissociation channels, these being C, S, CS, CS+C, CSS, and CSSC, and are shown in Fig. 4(a). The equation system mentioned earlier can then be expressed as the following:

$$N_C = T(1-T)N_{(14a)} + [T(1-T)^3 + T^2(1-T)^2 + T(1-T)^2]N_{(14c)}, \quad (15a)$$

$$N_S = [T(1-T)^3 + T^2(1-T)^2 + T(1-T)^2]N_{(14c)}, \quad (15b)$$

$$N_{CS} = [2T(1-T)^3 + 4T^2(1-T)^2 + 2T^3(1-T) + 4T(1-T)^2 + 4T^2(1-T) + 2T(1-T)]N_{(14b)} + [T(1-T)^3 + 2T^2(1-T)^2 + T^3(1-T) + T^2(1-T)]N_{(14c)}, \quad (15c)$$

$$N_{CS+C} = [2T^2(1-T)^2 + 2T^3(1-T) + T^2(1-T)]N_{(14c)}, \quad (15d)$$

$$N_{CSS} = T(1-T)N_{(14a)} + [T^2(1-T)^2 + T^3(1-T) + T^2(1-T)]N_{(14c)}, \quad (15e)$$

$$N_{CSSC} = T^2N_{(14a)} + [T^4 + 2T^3(1-T) + T^2(1-T)^2 + 2T^3 + 2T^2(1-T) + T^2]N_{(14b)} + [T^4 + T^3(1-T) + T^3]N_{(14c)} + [T^2 + T(1-T)]N_{(14d)}. \quad (15f)$$

The branching ratios α-δ are obtained from the following relationship:

$$\alpha\text{-}\delta = \frac{N_{(14a-14d)}}{N_{(14a)} + N_{(14b)} + N_{(14c)} + N_{(14d)}}. \quad (16)$$

The exothermic channels for N-methylacetamide-2,2,2-d_3 were derived using the data reported in Ref. 13,

$$CD_3COHNHCH_3^+ + e^-$$

$$\rightarrow CD_3COHNHCH_3 + H + 4.3 \text{ eV} \quad (17a)$$

$$\rightarrow CH_3NCCD_3 + H_2O + 8.8 \text{ eV} \quad (17b)$$

$$\rightarrow CH_3 + NH_2D + CD_2CO + 4.2 \text{ eV} \quad (17c1)$$

$$\rightarrow HOCNH + CH_3 + CD_3 + 0.7 \text{ eV} \quad (17c2)$$

$$\rightarrow CD_2CO + CH_3NH_2 + D + 3 \text{ eV} \quad (17d)$$

$$\rightarrow CH_3NH_2 + CD_3CO + 8.5 \text{ eV} \quad (17e)$$

$$\rightarrow HOCNH + C_2H_3D_3 + 4.5 \text{ eV} \quad (17f)$$

$$\rightarrow CD_3C(O)NH_2 + CH_3 + 5.1 \text{ eV} \quad (17g1)$$

$$\rightarrow CD_3C(OH)NH + CH_3 + 4.8 \text{ eV}. \quad (17g2)$$

The different mass peaks that can be observed from the above channels are 15, 18, 31, 33, 44, 46, 59, 62, and 75–77 Da. The masses produced from channels (17c1) and (17c2) are identical and hence these contributions are indistinguishable and have to be grouped together. This is also the case for channels (17g1) and (17g2). Furthermore, the peak intensities in the 75–77 Da mass region are very strong, making fits to these peaks impossible. As such, these peaks are considered as one peak in the analysis. The number of counts in each peak is then described by the following equation system:

$$\begin{pmatrix} N_{15} \\ N_{18} \\ N_{31} \\ N_{33} \\ N_{44} \\ N_{46} \\ N_{59} \\ N_{62} \\ N_{75-77} \end{pmatrix} = \begin{pmatrix} 0 & 0 & T(1-T)^2 & 0 & 0 & 0 & T(1-T) \\ 0 & T(1-T) & T(1-T)^2 & 0 & 0 & 0 & 0 \\ 0 & 0 & 0 & T(1-T)^2 & T(1-T) & 0 & 0 \\ 0 & 0 & T^2(1-T) & T(1-T) & 0 & T(1-T) & 0 \\ 0 & 0 & T(1-T)^2 & T(1-T)^2 & 0 & T(1-T) & 0 \\ 0 & 0 & 0 & T^2(1-T) & T(1-T) & 0 & 0 \\ 0 & T(1-T) & T^2(1-T) & 0 & 0 & 0 & 0 \\ 0 & 0 & T^2(1-T) & 0 & 0 & 0 & T(1-T) \\ T(1-T)+T^2 & T^2 & T^3 & T^3+T^2(1-T) & T^2 & T^2 & T^2 \end{pmatrix} \begin{pmatrix} N_{(17a)} \\ N_{(17b)} \\ N_{(17c)} \\ N_{(17d)} \\ N_{(17e)} \\ N_{(17f)} \\ N_{(17g)} \end{pmatrix}. \tag{18}$$

The branching ratios α-η are obtained in a similar fashion to that given in Eq. (16).

III. RESULTS AND DISCUSSION

A. Absolute cross section

1. DMDS

The cross section measured for protonated DMDS is plotted in Fig. 5. The contribution from unprotonated DMDS ions containing either the sulfur (^{33}S) or carbon isotopes (^{13}C) is estimated to be around 4.6% (intensity ratio $I_{m=95}/I_{m=94}\sim 0.7$). This contribution has been accounted for in the data analysis since the cross section for nonprotonated DMDS ion (94 Da) was measured as well. Differences in the shape and the magnitudes of the two cross sections were negligible. Similar effects were also observed in recent DR studies of $DCCCN^+$ and $DCCCND^+$ in Ref. 24.

2. N-methylacetamide-2,2,2-d_3

Figure 6 shows the measured DR cross section of protonated *N*-methylacetamide-2,2,2-d_3 over the energy range from 1 meV to 0.3 eV. For this ion the contribution from the radical cation due to the ^{13}C isotope was less than 0.3% and therefore was neglected.

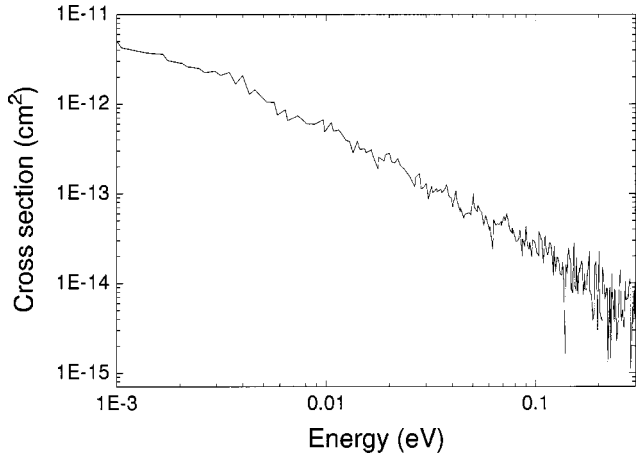

FIG. 5. The measured DR cross section of protonated DMDS for center-of-mass collision energies between 1 meV and 0.3 eV.

The thermal rate coefficient for both protonated *N*-methylacetamide-2,2,2-d_3 and protonated DMDS was found to be 1.86×10^{-6} and 1.48×10^{-6} cm^3/s at electron temperature 300 K, respectively.

There are two types of errors that are represented in the value of the cross section. The first error is a systematic error which is due to the uncertainties in the ion and electron current measurement and the ion-electron interaction length. This error is estimated to be around 10%. The second error is statistical error which varies from 0.5% at 1 meV collision energy to ~15% at 0.3 eV collision energy. This variation is due to the DR count rate which is much higher at low collision energies.

B. Branching ratios

1. DMDS

The calculated DR branching ratios for protonated DMDS are given in Table II. The production of a methyl fragment is the dominant reaction with 62.5%, while S-S bond cleavage is only 9.8%. This should be compared with the results of a neutralization-reionization study which showed cleavage of the C-H, C-S, and S-S bonds.[10] The fact that protonated dimethyl disulfide is not preferentially

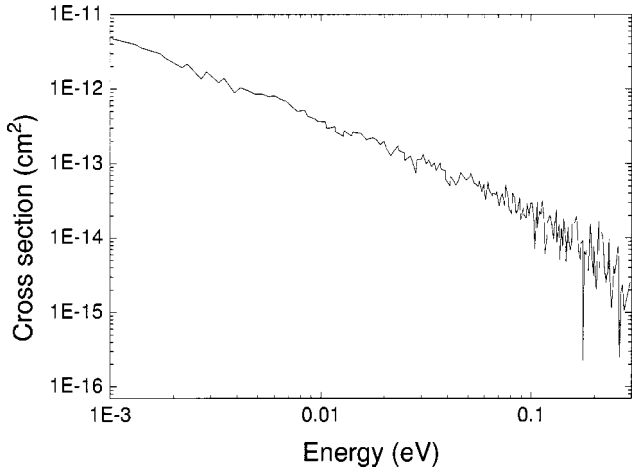

FIG. 6. The measured DR cross section of protonated *N*-methylacetamide-2,2,2-d_3 for center-of-mass collision energies between 1 meV and 0.

TABLE II. Dissociative recombination branching ratios of protonated DMDS for 0 eV center-of-mass collision energy.

Dissociation channel (channel number)	Branching (%)
CSS+C (14a)	62.5±0.9
CS+CS (14b)	9.8±0.3
C+S+CS (14c)	22.3±1.0
CSSC (14d)	5.4±2.1

cleaved at the S-S bond is apparently in contrast to the fact that ECD induced S-S bond cleavage is so prominent in proteins. The most likely explanation seems to be that disulfides are not protonated to any extent in proteins. This is in line with a recent theoretical survey which concluded that the two most likely mechanisms appear to be either spontaneous dissociation of the S-S bond upon impact of slowly moving free hydrogen or induced by uptake of a nascent hydrogen radical initially in close contact through a hydrogen bond.[11,12] As already mentioned the complete DR branching cannot be measured due to technical reasons. As such we cannot obtain, for instance, the separate contributions of channels (13c) and (13d) to channel (14c).

2. N-methylacetamide-2,2,2-d_3

Table III summarizes the branching of *N*-methylacetamide-2,2,2-d_3. The dominant reaction channel (81.7%) involves the production of a single hydrogen atom. Interestingly, products due to N-C_α bond cleavage account for about 7% while no products arising from peptide bond cleavage were observed. This result is in good agreement with the neutralization-reionization study of protonated *N*-methylacetamide-2,2,2-d_3 (Ref. 13), who found a preference of H loss (from the oxygen) to CH_3 loss (from the nitrogen) in the ratio 1.7:1. Their corresponding *ab initio* model was in accordance with this. Both the present findings and those of Ref. 13 agree with the fact that upon ECD, protonated peptides preferentially break at the N-C_α bond, but also that they easily give off the proton in the form of a hydrogen atom. If these hydrogens are captured by other functional groups in the protein, a disulfide or another peptide bond, these may become activated for cleavage.

TABLE III. Dissociative recombination branching ratios of protonated *N*-methylacetamide for 0 eV center-of-mass collision energy.

Dissociation channel (channel number)	Branching (%)
$CD_3COHNHCH_3+H$ (17a)	81.7±1.1
$CH_3NCCD_3+H_2O$ (17b)	4.2±0.3
$CH_3+NH_2D+CD_2CO$ (17c1) and $HOCNH+CH_3+CD_3$ (17c2)	0.2±0.1
$CD_2CO+CH_3NH_2+D$ (17d)	0
$CH_3NH_2+CD_3CO$ (17e)	1.8±0.5
$HOCNH+C_2H_3D_3$ (17f)	6.3±1.1
$CD_3C(O)NH_2+CH_3$ (17g1) and $CD_3C(OH)NH+CH_3$ (17g2)	6.8±0.3

IV. CONCLUSION

The DMDS and the *N*-methylacetamide molecules are two first choice model systems that represent the disulfide bridge bond and the peptide bond in proteins. These systems are therefore suitable for investigation of the mechanisms involved when proteins fragment under ECD. The DR cross sections of the protonated DMDS and *N*-methylacetamide-2,2,2-d_3 were measured for collision energies from 1 meV to 0.3 eV. No high-energy structure was observed in the cross sections for collision energies up to 16 eV. The obtained DR thermal rate of DMDS is of the same order of magnitude as that obtained for protonated *N*-methylacetamide-2,2,2-d_3. This indicates that S-S bond cleavage, which is observed as the dominant reaction in the ECD process, is not likely the result of a direct electron capture by the (unfavored) protonated disulphide bridge.

The DR branching ratios at 0 eV collision energy were measured for the protonated molecules of DMDS and *N*-methylacetamide-2,2,2-d_3. Cleaving the CSS-C bond was found to be the most dominant channel (62.5%) in the protonated DMDS. The dominant channel (81.7%) for recombination of protonated *N*-methylacetamide-2,2,2-d_3 is the production of a hydrogen atom. This strongly suggests that protonated proteins may release hydrogens upon ECD, and that some of the cleavages observed are hydrogen capture induced. A similar argument, related to the high hydrogen affinity of the disulphide bridge, may also explain why fragments arising from S-S bond cleavages are observed in the ECD spectra of proteins.

Despite the beauty of these simple model systems, we must realize their (literally speaking) shortcomings. The size and complexity of proteins with their entangled chains, large number of degrees of freedom, and internal solvation and hydrogen bonding are of significance in their chemical behavior as observed in ECD. A realistic molecular model should not only encompass the minimum criteria of containing the right functional groups but must also take intramolecular interactions properly into account. For example, the existence of intramolecular hydrogen binding seems to be pivotal in the detailed dynamics of dissociation, in particular by providing a channel for nonergodic dissociation, a feature also observed in ECD.[14] Having said so, the present results definitely give support for the indirect mechanism in which thermal hydrogens play a central role. The picture which emerges is that the direct and indirect mechanisms work in parallel.

ACKNOWLEDGMENTS

This work was supported by the European Community's Research Training Networks Program under Contract Nos. HPRN-CT-2000-0142 and HPMF-CT-2002-01583. The authors wish to thank VR (The Swedish Research Council) for their financial support. E.U, J.V., and C.A. wish to thank NFR (The Norwegian Research Council) for financial support through a postdoctoral fellowship for C.A. J.S. and M.K. acknowledge support in part by the State Committee for Scientific Research, Poland. We are also grateful for a

generous grant of computing time from NOTUR (The Norwegian High Performance Computing Consortium).

[1] R. A. Zubarev, N. L. Kelleher, and F. W. McLafferty, J. Am. Chem. Soc. **120**, 3265 (1998).
[2] R. A. Zubarev, N. A. Kruger, E. K. Fridriksson, M. A. Lewis, D. M. Horn, B. K. Carpenter, and F. W. McLafferty, J. Am. Chem. Soc. **121**, 2857 (1999).
[3] N. A. Kruger, R. A. Zubarev, D. M. Horn, and F. W. McLafferty, Int. J. Mass. Spectrom. **185–187**, 787 (1999).
[4] N. A. Kruger, R. A. Zubarev, B. K. Carpenter, N. L. Kelleher, D. M. Horn, and F. W. McLafferty, Int. J. Mass Spectrom. Ion Processes **182–183**, 1 (1999).
[5] R. A. Zubarev, D. M. Horn, E. K. Fridriksson, N. L. Kelleher, N. A. Kruger, M. A. Lewis, B. K. Carpenter, and F. W. McLafferty, Anal. Chem. **72**, 1 (2000).
[6] P. Roepstorff and J. Fohlman, Biomed. Mass Spectrom. **11**, 601 (1984).
[7] J. A. Loo, H. R. Udseth, and R. D. Smith, Rapid Commun. Mass Spectrom. **2**, 207 (1988).
[8] J. W. Gauthier, T. R. Trauman, and D. B. Jacobsen, Anal. Chim. Acta **246**, 211 (1991).
[9] M. W. Senko, J. P. Speir, and F. W. McLafferty, Anal. Chem. **66**, 2801 (1994).
[10] F. Tureček, M. Polášek, A. J. Frank, and M. Sadilek, J. Am. Chem. Soc. **122**, 2361 (2000).
[11] A. Sawicka, P. Skurski, R. R. Hudgins, and J. Simons, J. Phys. Chem. B **107**, 13505 (2003).
[12] E. Uggerud, Int. J. Mass. Spectrom. **234**, 45 (2004).
[13] E. A. Syrstad, D. D. Stephens, and F. Tureček, J. Phys. Chem. A **107**, 115 (2003).
[14] V. Bakken, T. Helgaker, and E. Uggerud (unpublished).
[15] M. Larsson, Adv. Gas-Phase Ion Chem. **4**, 179 (2001).
[16] A. Al-Khalili, S. Rosén, H. Danared *et al.*, Phys. Rev. A **68**, 042702 (2003).
[17] A. Neau, A. Al-Khalili, S. Rosén *et al.*, J. Chem. Phys. **113**, 1762 (2000).
[18] J. R. Peterson, A. Le Padellec, H. Danared *et al.*, J. Chem. Phys. **108**, 1978 (1998).
[19] H. Danared, G. Andler, L. Bagge *et al.*, Phys. Rev. Lett. **72**, 3775 (1994).
[20] A. Paal, A. Simonsson, A. Källberg, J. Dietrich, and I. Mohos, *6th European Workshop on Beam Diagnostics and Instrumentation for Particle Accelerators* (Darmstadt, 2003), pp. 240–241 (available online: http://bel.gsi.de/dipac2003/).
[21] M. J. Frisch, G. W. Trucks, H. B. Schlegel *et al.*, GAUSSIAN 98, Gaussian Inc., Pittsburgh, PA, 1998.
[22] A. P. Scott and L. Radom, J. Phys. Chem. **100**, 16502 (1996).
[23] L. A. Curtiss, K. Raghavachari, G. W. Trucks, and J. A. Pople, J. Chem. Phys. **94**, 7221 (1991).
[24] W. D. Geppert, A. Ehlerding, F. Hellberg *et al.* (unpublished).